Coupled 3D Time-Dependent Wave-Packet Approach in Hyperspherical Coordinates: The D(+)+H2 Reaction on the Triple-Sheeted DMBE Potential Energy Surface

ARTICLE *in* THE JOURNAL OF PHYSICAL CHEMISTRY A · OCTOBER 2015

Impact Factor: 2.69 · DOI: 10.1021/acs.jpca.5b07718

5 AUTHORS, INCLUDING:

Tapas Sahoo

Weizmann Institute of Science

13 PUBLICATIONS **41** CITATIONS

SEE PROFILE

Rahul Sharma

St. Xavier's College, Kolkata

24 PUBLICATIONS **124** CITATIONS

SEE PROFILE

Antonio J. C. Varandas

University of Coimbra

382 PUBLICATIONS **6,747** CITATIONS

SEE PROFILE

THE JOURNAL OF PHYSICAL CHEMISTRY A

Article

pubs.acs.org/JPCA

Coupled 3D Time-Dependent Wave-Packet Approach in Hyperspherical Coordinates: The D^++H_2 Reaction on the Triple-Sheeted DMBE Potential Energy Surface

Sandip Ghosh,[†] Tapas Sahoo,[‡] and Satrajit Adhikari*[,†]

[†]Department of Physical Chemistry, Indian Association for the Cultivation of Science, 2A & 2B Raja S. C. Mullick Road, Jadavpur, Kolkata-700032, West Bengal, India

[‡]Weizmann Institute of Science, 234 Herzl Street, Rehovot, Illinois 7610001, Israel

Rahul Sharma[§] and António J. C. Varandas*

Departamento de Química, and Centro de Química, Universidade de Coimbra, 3004-535 Coimbra, Portugal

Supporting Information

ABSTRACT: We implement a coupled three-dimensional (3D) time-dependent wave packet formalism for the 4D reactive scattering problem in hyperspherical coordinates on the accurate double many body expansion (DMBE) potential energy surface (PES) for the ground and first two singlet states ($1^1A'$, $2^1A'$, and $3^1A'$) to account for nonadiabatic processes in the $D^+ + H_2$ reaction for both zero and nonzero values of the total angular momentum (J). As the long-range interactions in $D^+ + H_2$ contribute significantly due to nonadiabatic effects, the convergence profiles of reaction probabilities for the reactive noncharge transfer (RNCT), nonreactive charge transfer (NRCT), and reactive charge transfer (RCT) processes are shown for different collisional energies with respect to the helicity (K) and total angular momentum (J) quantum numbers. The total and state-to-state cross sections are presented as a function of the collision energy for the initial rovibrational state $v = 0$, $j = 0$ of the diatom, and the calculated cross sections compared with other theoretical and experimental results.

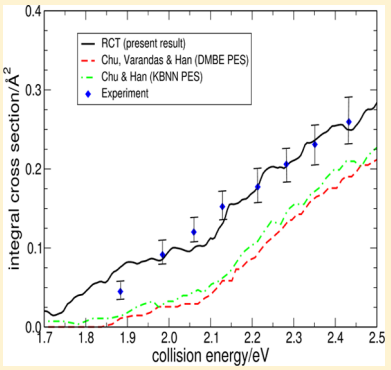

I. INTRODUCTION

Exact quantum mechanical calculations of triatomic systems for collinear[1−8] arrangements had been endeavored a long way back. Kuppermann, Schatz, and Baer[9] pioneered the development of the accurate methodology to solve the Schrödinger equation for triatomic reactions on a single Born−Oppenheimer (BO) PES. At that time, there were theoretical approaches being investigated, namely, the R-matrix propagation,[10] use of hyperspherical coordinates,[11−15] the S-matrix formulation,[16−18] and approaches based on the Newton-variational-principle.[19,20] Rovibrationally resolved state-to-state integral and differential cross sections of triatomic reactions were assessed by significant experimental advances[21−25] on precise product detection techniques, which led to venture both time-independent and time-dependent methodologies to elucidate those results.[26−28]

The time-dependent wave packet approaches were primarily formulated in Jacobi coordinates for the initial state-resolved total reaction probabilities[29] and cross sections[30] for $J = 0$ only, with the results for $J \neq 0$ being not as accurate as the corresponding time-independent ones due to the inherent reactant−product coordinate transformation problem. There were several efforts to transform the coordinates as the wave packet reaches the strong interaction region,[31,32] but those emerged to be either expensive or inaccurate. Essentially, Zhang and co-workers[33] had overcome the problem by introducing the so-called "reactant-product decoupling" (RPD) scheme, which was transmuted by Kouri and co-workers.[34−36] Later on, Althorpe and co-workers[37−41] formulated an efficient algorithm to calculate accurate and fully converged initial sate resolved integral and differential cross sections even for $J \neq 0$. In turn, Gray and Balint-Kurti[42] developed an accurate time-dependent quantum dynamics method with real wave packets for reactive scattering to calculate atom plus diatom integral and differential cross sections. Recently, several other time-dependent approaches have been employed for calculation of reaction probability as well as integral and differential cross sections on various triatomic reactive systems.[43−46] In addition, state-to-state reactive scattering calculations for triatomic systems have been performed using a dynamics code on graphics processing units (GPUs).[47]

Special Issue: Dynamics of Molecular Collisions XXV: Fifty Years of Chemical Reaction Dynamics

Received: August 8, 2015
Revised: October 1, 2015

DOI: 10.1021/acs.jpca.5b07718
J. Phys. Chem. A XXXX, XXX, XXX−XXX

The awkward problem of coordinate transformation from reactant to product channel was avoided by implementing the Coupled Channel (CC) approach in hyperspherical coordinates[48−63] which can resolve the problem by smoothly changing the frame of reference from the reactants, A + BC, to the products, AC + B and AB + C. Accurate state-to-state cross sections and reaction probabilities have been produced in the recent past for a variety of triatomic reactions by using the Coupled Channel (CC) approach in hyperspherical coordinates with the computational cost scaling as $(J\prod N_i)^3$ with increasing total angular momentum (J) and number of basis functions used for the ith internal coordinate (N_i). On the other hand, the time-dependent wave packet approach in hyperspherical coordinates makes itself convenient for an equivalent description of all rearrangement channels, while the computational demand of the grid method scales as $J\prod_i N_i \sum_i \log N_i$.

Since any triatomic reaction is a 4D quantum mechanical problem, it is feasible to formulate its "exact" solution in terms of coupled 3D wave packets expressed in terms of the hyperradius (ρ) and hyperangles (θ and ϕ), and the K-component waves, where K is the helicity quantum number. Billing and co-workers[62,63] formulated this approach using hypersperical coordinates to perform 3D as well as coupled 3D wave packet calculations for the D + H_2 system in the simplest cases of J = 0 and J = 1. Recently, Adhikari and Varandas[48] implemented this formulation to carry out time-dependent wave packet calculations on triatomic systems both for J = 0 and $J \neq 0$ situations. A while later, Crawford and Parker[64] went on to compute state-to-state three-atom time-dependent reactive scattering in hyperspherical coordinates for H + H_2 and F + H_2 with J = 0. The workability of our OpenMP-MPI parallelized algorithm[49] has also been explored for the D^+ + H_2 reaction on the lowest adiabatic singlet ($1^1A'$) sheet for collision energies between 1.7 and 2.5 eV. Further investigation of our dynamics code[50] using the same PES has also been done in the low energy regime, where the process is truly adiabatic in nature and consequently charge transfer processes are not expected to occur. State-to-state as well as total cross sections and rate coefficients for the reactive noncharge transfer (RNCT) process have been calculated, where the reaction probabilities as a function of number of the K-waves, cross section as a function of collision energy, and temperature-dependent rate coefficients are reported.[49,50] In spite of the difficulties of time-dependent methodologies in the very low energy regime, the calculated rate constants are shown to be in good agreement with the experimental ones.[65,66] As the ground- and first-excited singlet states have avoided crossings, multisurface calculations are required at high energy regimes (1.7−2.5 eV) in order to obtain results that may be compared with existing experimentally measured ones.[67]

Due to so-called molecular simplicity and importance in interstellar chemistry, H_3^+ has been the benchmark system for both experimental and theoretical studies. Despite its relative simplicity, exact quantum mechanical calculations are very difficult due to the extraordinary deep well (∼4.0 eV) appearing in the reaction path. Moreover, it is clearly seen from recent theoretical calculations[68−70] that the charge transfer processes occurring on multiple PESs have been the center of attention in the nonadiabatic dynamics. Indeed, the competing reactive and nonreactive processes involving charge transfer on multiple PESs have motivated a lot of theoretical studies on this system. Since theoretical and experimental findings for the transition probabilities and cross sections are available, the primary incentive of the present work is to investigate the workability of our methodology[48−50] using the multisheeted DMBE PES. Integral cross sections for the reaction H^+ + D_2 were scanned by the guided beam experimental technique,[71] where the rate constants[72] at various collision energies were acquired for the ion-atom exchange reactions H^+ + D_2 and D^+ + H_2. On the other hand, drift tube experiments[73] have been carried out for the reactions H^+ + D_2 → HD + D^+ and D^+ + H_2→ HD + H^+ in the energy range 0.04−0.3 eV. Moreover, a temperature-variable selected ion flow-tube technique[74] was able to measure the forward and reverse rate constants at 205 and 295 K. In turn, Gerlich[66] employed the merged beams technique to estimate rate coefficients for D^+ + (normal)H_2 from 180 to 350 K, where reaction cross sections were measured for collisional energies down to the 1 meV magnitude. In order to understand the mechanism of these processes, many theoretical calculations on approximate[75,76] and accurate[68,69,77−79] PESs have been performed. Though the most recent and accurate diabatic PESs for the singlet states of the H_3^+ system are constructed[70] by employing *ab initio* calculated nonadiabatic coupling terms with the help of beyond Born−Oppenheimer theories,[80] at present we perform dynamical calculations on the diabatic surfaces developed by Varandas and co-workers.[69] Since such diabatic surfaces[69] are used by other dynamical approaches[81] and the results are available for comparison, we explore the workability of our dynamical code in hyperspherical coordinates for multisurface cases.

For high-energy regimes, time-dependent and time-independent 3D quantum scattering[68,82−84] calculations in hyperspherical coordinates were executed on three diabatic surfaces constructed by the Diatomics-In-Molecules (DIM) approach and fitted to *ab initio* data to explore the effect of nonadiabaticity in the D^+ + H_2 reaction at J = 0. On the other hand, time-independent scattering[68,83,85,86] and time-dependent wave packet[81,87−89] calculations have also been investigated for the same energy range using *ab initio* calculated diabatic PESs considering both the centrifugal sudden (CS) and close coupled (CC) methodologies with nonzero total angular momenta. Some other essential details of the H_3^+ charge transfer and non charge transfer processes are highlighted in the recent review articles.[90−92] In summary, we investigate three channels, namely, reactive noncharge transfer (RNCT), nonreactive charge transfer (NRCT), and reactive charge transfer (RCT):

$$D^+ + H_2 \rightarrow DH + H^+ \quad \text{RNCT}$$

$$D^+ + H_2 \rightarrow D + H_2^+ \quad \text{NRCT}$$

$$D^+ + H_2 \rightarrow DH^+ + H \quad \text{RCT}$$

For this, we have employed the multisheeted singlet DMBE PES ($1^1A'$, $2^1A'$, and $3^1A'$)[69] of H_3^+, thus scrutinizing the competence of our quantum dynamics methodology[48−50] in hyperspherical coordinates to handle any nonzero total angular momenta over the collision energy range 1.7−3.0 eV. The workability of our approach will then be demonstrated by convergence profiles of the calculated reaction probabilities as a function of the helicity quantum number (K) and total angular momentum (J). State-to-state and total cross sections will also be reported over a range of collision energies.

DOI: 10.1021/acs.jpca.5b07718
J. Phys. Chem. A XXXX, XXX, XXX−XXX

II. THEORETICAL BACKGROUND

The (nonreactive/reactive) asymptotic solution for triatomic reactive scattering in Jacobi coordinates may be written as

$$\Psi \rightarrow \frac{1}{Rr} \sum_{\gamma' vjl} u^{Jl'}_{\gamma\gamma'}(R) y^{JM}_{jl}(\hat{R}, \hat{r}) \phi_{vj}(r) \tag{1}$$

where γ, γ' denote the quantum numbers for the incoming wave packet of the atom, J is the total angular momentum of the triatom with projection quantum numbers M, l and l' are the orbital angular momentum of the same triatom, and j is the rotational quantum number of the diatom. The functions y^{jl}_{JM} and ϕ_{vj} are Arthurs−Dalgarno (AD)[93] and vibrational states, respectively. The vibrational wave packet ϕ_{vj} depends upon the rotational quantum number j through the centrifugal coupling term. The volume element of such a wave function is given by

$$R^2 dR r^2 dr \sin\Theta' d\Theta' d\Phi' \sin\eta d\eta d\xi \tag{2}$$

Note that the separation between the atom (A) and the center of mass of the diatomic molecule (BC) is considered to be R, whereas Θ' and Φ' represent its orientation in space-fixed coordinates (see Figure 1). Similarly, the bond distance of the BC molecule is taken to be r, where the angles η and ξ specify its orientation in a body-fixed coordinate system.

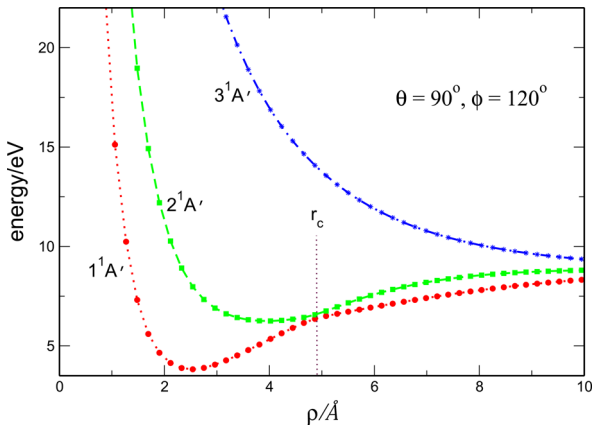

Figure 1. Energy profiles of the ground and first two excited states.

The wave packet on the adiabatic PES can be initialized in Jacobi coordinates as

$$\psi^a = \sqrt{\sin\eta\, J(R\eta|\rho\theta\phi)}\, \phi_{vj}(r) y^{JM}_{jl} \chi(R) \tag{3}$$

where the orientation angle (η) of the diatom and the Jacobian ($J(R\eta|\rho\theta\phi)$) for the transformation are defined by

$$\sin\eta = \frac{\cos\theta}{\sqrt{1 - \sin^2\theta \cos^2\phi}} \tag{4}$$

and

$$J(R\eta|\rho\theta\phi) = \frac{\rho}{2} \frac{\sin\theta}{\sqrt{1 - \sin^2\theta \cos^2\phi}} \tag{5}$$

respectively.

Moreover, the wave packet ψ^a in eq 3 can be expressed in terms of the Wigner **D** matrix and K-component wave function ($\Phi^a_K(\rho, \theta, \phi)$):

$$\psi^a = \sum_{K=-J}^{J} \Phi^a_K(\rho, \theta, \phi) \sqrt{\frac{2J+1}{8\pi^2}} D^{J*}_{MK}(\alpha, \beta, \gamma) \tag{6}$$

where $\sqrt{\frac{2J+1}{8\pi^2}} D^J_{MK}$ is normalized on $d\alpha \sin\beta\, d\beta d\gamma$ and α, β, and γ denote the Euler angles. Thus, the normalization of the wave packet in terms of K-component waves becomes

$$\sum_K \int d\rho d\theta d\phi |\Phi^a_K|^2 = 1 \tag{7}$$

Taking eqs 3 and 6 into account, the compact form of the wave packet in hyperspherical coordinates in terms of 3−j symbols and modified spherical harmonics ($C_{j\mu}$) leads to

$$\Phi^a_K = \sqrt{2\pi \sin\eta J(R\eta|\rho\theta\phi)(2l+1)}\, \phi_{vj}(r) \chi(R) (-1)^{j-l} \times \sum_\mu \begin{pmatrix} j & l & J \\ \mu & 0 & -\mu \end{pmatrix} C_{j\mu}(\eta) A_{K\mu} \tag{8}$$

where

$$A_{K\mu} = (-1)^K \int_0^{2\pi} d\gamma \int_0^{\pi} d\beta \sin\beta \times \exp(-iK\gamma + i\mu\xi) C_{JK}(\beta) C_{J\mu}(\Theta') \tag{9}$$

which obeys the orthonormality condition:

$$\sum_K A^*_{K\mu} A_{K\mu'} = \delta_{\mu\mu'} \tag{10}$$

In terms of Johnson's hyperspherical coordinates,[94] the diabatic Hamiltonian operator related with the three-particle system is expressed as

$$\hat{H} = \left\{ -\frac{\hbar^2}{2\mu_R} \frac{\partial^2}{\partial\rho^2} + \frac{2}{\mu_R \rho^2} \hat{L}^2(\theta, \phi) + \frac{\hat{J}^2 - \hat{J}_z^2}{\mu_R \rho^2 \cos^2\theta} + \frac{\hat{J}_z^2 - 4\cos\theta \hat{J}_z \hat{P}_\phi}{2\mu_R \rho^2 \sin^2\theta} + \frac{\sin\theta}{\mu_R \rho^2 \cos^2\theta} \frac{1}{2} [\hat{J}_+^2 + \hat{J}_-^2] \right\} \hat{I} + \hat{V}_0(\rho, \theta, \phi) \tag{11}$$

where

$$\hat{J}_z = -i\hbar \left(\frac{\partial}{\partial\gamma} \right) \tag{12}$$

$$\hat{P}_\phi = -i\hbar \left(\frac{\partial}{\partial\phi} \right) \tag{13}$$

$$\hat{L}^2(\theta, \phi) = -\hbar^2 \left[\frac{\partial^2}{\partial\theta^2} + \frac{1}{\sin^2\theta} \frac{\partial^2}{\partial\phi^2} \right] \tag{14}$$

$$\hat{V}_0(\rho, \theta, \phi) = \begin{bmatrix} V_{11} + \Delta V & V_{12} & V_{13} \\ V_{21} & V_{22} + \Delta V & V_{23} \\ V_{31} & V_{32} & V_{33} + \Delta V \end{bmatrix} \tag{15}$$

DOI: 10.1021/acs.jpca.5b07718
J. Phys. Chem. A XXXX, XXX, XXX−XXX

$$\Delta V(\rho, \theta) = -\frac{\hbar^2}{2\mu_R \rho^2}\left[\frac{1}{4} + \frac{4}{\sin^2 2\theta}\right] \tag{16}$$

$$\mu_R = \sqrt{\frac{m_A m_B m_C}{m_A + m_B + m_C}} \tag{17}$$

Thus, $\hat{I}$ is a unit matrix, $\hat{V}_0$ denotes the (3 × 3) interaction potential matrix for the triatomic system, and $\hat{J}_+$, $\hat{J}_-$ are the raising and lowering operators, respectively. We transform the adiabatic K-component wave function ($\Phi^a_{K,I}$) for different surfaces (I = 1, 2, 3) to the diabatic ones ($\Phi^d_{K,I}$) by using the matrix that diagonalizes $\hat{V}_0(\rho, \theta, \phi)$. By substituting the wave functions $\Phi^d_{K,I}$ and the Hamiltonian [eq 11] into the time-dependent Schrödinger equation (TDSE), one can obtain the following set of coupled equations in terms of K-component waves ($\Phi^d_{K,I}$) for each surface:

$$i\hbar\frac{\partial}{\partial t}\begin{bmatrix}\Phi^d_{K,1}\\ \Phi^d_{K,2}\\ \Phi^d_{K,3}\end{bmatrix} = \left\{-\frac{\hbar^2}{2\mu_R}\frac{\partial^2}{\partial\rho^2} + \frac{2}{\mu_R\rho^2}\hat{L}^2(\theta, \phi)\right.$$
$$+ \frac{\hbar K(\hbar K - 4\cos\theta\,\hat{P}_\phi)}{2\mu_R\rho^2\sin^2\theta}$$
$$\left. + \frac{\hbar^2[J(J+1) - K^2]}{\mu_R\rho^2\cos^2\theta} + \Delta V(\rho, \theta)\right\}\begin{bmatrix}\Phi^d_{K,1}\\ \Phi^d_{K,2}\\ \Phi^d_{K,3}\end{bmatrix}$$
$$+ \begin{bmatrix}V_{11} + \Delta V & V_{12} & V_{13}\\ V_{21} & V_{22} + \Delta V & V_{23}\\ V_{31} & V_{32} & V_{33} + \Delta V\end{bmatrix}\begin{bmatrix}\Phi^d_{K,1}\\ \Phi^d_{K,2}\\ \Phi^d_{K,3}\end{bmatrix}$$
$$+ \frac{\sin\theta}{\mu_R\rho^2\cos^2\theta}\left(M_{K,K+2}\begin{bmatrix}\Phi^d_{K+2,1}\\ \Phi^d_{K+2,2}\\ \Phi^d_{K+2,3}\end{bmatrix} + M_{K,K-2}\begin{bmatrix}\Phi^d_{K-2,1}\\ \Phi^d_{K-2,2}\\ \Phi^d_{K-2,3}\end{bmatrix}\right) \tag{18}$$

where the diabatic wave functions $\Phi^d_{K,I}$ and $\Phi^d_{K\pm2,I}$ are coupled via the coupling element:

$$M_{K,K\pm2} = \frac{\hbar^2}{2}\sqrt{(J \mp K)(J \pm K + 1)(J \mp K - 1)(J \pm K + 2)} \tag{19}$$

The K-component waves $\Phi^d_{K,I}(\rho, \theta, \phi)$ are represented in a discrete way on three-dimensional grids in order to propagate the coupled wave packets in time.

We project the time-dependent wave packet onto asymptotic eigenstates at a fixed value of R which makes the asymptotic propagation part of the problem even simpler to handle.[62,63] The scattering amplitude in the channel specified by vibrational, rotational, and orbital quantum numbers v', j', l' for different surfaces (I = 1, 2, 3) can be evaluated as follows:

$$u^{J,I}_{v'j'l'}(R; t) = 4R\int dr\int d\eta r\,\sin\eta\rho^{-5/2}(\sin 2\theta)^{-1/2}\phi^I_{v'j'}(r) \times\sum_{K\mu'} g_{j'l'\mu'}A^*_{K\mu'}C_{j'\mu'}(\eta)\Phi^a_{K,I}(\rho, \theta, \phi) \tag{20}$$

where the adiabatic K-component wave functions ($\Phi^a_{K,I}$) are transformed back from the diabatic ones ($\Phi^d_{K,I}$) at each time step of propagation and $\phi^I_{v'j'}$ is a vibrational eigenfunction corresponding to the adiabatic state. The modified constant for the 3−j symbol is defined as

$$g_{jl\mu} = \sqrt{2\pi(2l+1)}\,(-1)^{j-l}\begin{pmatrix} j & l & J\\ \mu & 0 & -\mu\end{pmatrix} \tag{21}$$

The integration is performed over the (θ, ϕ) grid using the relations:

$$\rho = \sqrt{2}\,d_i R/\sqrt{1 - \sin\theta\cos(\phi - \epsilon_i)} \tag{22}$$

$$r = \frac{d_i\rho}{\sqrt{2}}\sqrt{1 + \sin\theta\cos(\phi - \epsilon_i)} \tag{23}$$

$$\sin\eta = \cos\theta/\sqrt{1 - \sin^2\theta\cos^2(\phi - \epsilon_i)} \tag{24}$$

with the Jacobi factor (for fixed R) given by

$$J(r, \eta|\theta, \phi) = \frac{d_i^2 R\sin\theta}{[1 - \sin\theta\cos(\phi - \epsilon_i)]\sqrt{1 - \sin^2\theta\cos^2(\phi - \epsilon_i)}} \tag{25}$$

where d_i and ϵ_i are channel-dependent constants.

The outgoing wave packet is projected onto asymptotic eigenstates at a relatively large value of the Jacobi coordinate R = R* in order to neglect the coupling. Since the projection is performed for a fixed value of asymptotic R and the amplitude of the K-waves ($\Phi^a_{K,I}$) is a function of ρ, θ, and ϕ, we interpolate the amplitudes of the K-component waves on the grid to acquire the corresponding value of $\Phi^a_{K,I}$ on (θ, ϕ)-space at R = R*.

After the wave packet passes through the projection region and gets absorbed at the boundary, the scattering amplitudes are Fourier transformed from time to energy space, leading to

$$b^{J,I}_{v'j'l'}(E; R) = \frac{1}{\sqrt{2\pi}}\int dt u^{J,I}_{v'j'l'}(R; t)\exp(iEt/\hbar) \tag{26}$$

These amplitudes are then expanded in terms of incoming and outgoing waves as

$$b^{J,I}_{v'j'l'} = A^{in}_{v'j'l'}k_{v'j'}Rh^-(k_{v'j'}R) + A^{out,I}_{v'j'l'}k_{v'j'}Rh^+(k_{v'j'}R) \tag{27}$$

where

$$h^\pm(k_{v'j'}R) = -n_l(k_{v'j'}R) \pm ij_l(k_{v'j'}R) \tag{28}$$

and j_l and n_l are spherical Bessel and Neumann functions, respectively. Of course, after collision, at asymptotic time, the projection on the incoming component of the scattering amplitude ($A^{in}_{v'j'l'}$) should be zero.

The amplitudes corresponding to the asymptotic product states are obtained by performing a transformation from the unique adiabatic to the approximate diabatic representation. This is easily done asymptotically since

DOI: 10.1021/acs.jpca.5b07718
J. Phys. Chem. A XXXX, XXX, XXX−XXX

$$\Phi^d_{K,1} = \Phi^a_{K,1}, \quad r < r_c$$
$$\Phi^d_{K,1} = \Phi^a_{K,2}, \quad r \geq r_c$$
$$\Phi^d_{K,2} = \Phi^a_{K,2}, \quad r < r_c$$
$$\Phi^d_{K,2} = \Phi^a_{K,1}, \quad r \geq r_c \tag{29}$$

where the indices 1 and 2 correspond to neutral (H_2) and ionic (H_2^+) products, respectively, and r_c denotes the bond length where the crossing of these two diabatic potential curves occurs (see Figure 3). The scattering amplitudes corresponding to this diabatic representation are then evaluated as

$$d^1_{v',j',l'} = \sum_v \{b^{J,1}_{v,j',l'} Ol^{11}_{v,v',j'} + b^{J,2}_{v,j',l'} Or^{21}_{v,v',j'}\}$$
$$d^2_{v',j',l'} = \sum_v \{b^{J,2}_{v,j',l'} Ol^{22}_{v,v',j'} + b^{J,1}_{v,j',l'} Or^{12}_{v,v',j'}\} \tag{30}$$

where Ol and Or are vibrational matrix elements:

$$Ol^{II'}_{v,v',j'} = \int_0^{r_c} \phi^I_{vj} \phi^{I'}_{v'j'},$$
$$Or^{II'}_{v,v',j'} = \int_{r_c}^{\infty} \phi^I_{vj} \phi^{I'}_{v'j'}. \tag{31}$$

The reaction probability from the initial state (vjl) to the product state ($v'j'l'$) on the I^{th} surface could be calculated as the ratio of the outgoing and incoming fluxes,

$$P^I_{v'j'l' \leftarrow vjl} = \frac{F^I_{v'j'l'}}{F_{vjl}} \tag{32}$$

where

$$F^I_{v'j'l'} = \frac{1}{\mu_{out}} k_{v'j'} |d^I_{v',j',l'}|^2 \tag{33}$$

$$F_{vjl} = \frac{1}{\mu_{in}} k_{vj} |c^l_E|^2 \tag{34}$$

In the above equations, c^l_E is the scattering amplitude of the initial wave packet at energy E, and k_{vj}, $k_{v'j'}$ are the wave vectors of the initial (vj) and final ($v'j'$) channels, respectively, and μ_{in} and μ_{out} are the appropriate triatomic centers of mass for the reactants and products, respectively. The weights of the scattering amplitudes in energy (E) and wave vector (k) space are related as

$$|c^l_E|^2 = \left(\frac{\mu_{in}}{\hbar k}\right)^2 |c^l_k|^2 \tag{35}$$

where the analytic expression of $|c^l_k|^2$ for a Gaussian wave packet can be obtained as

$$|c^l_k|^2 = \sqrt{2/\pi}\,\sigma \exp[-2\sigma^2(k - k_0)^2] \tag{36}$$

with σ being the width of the Gaussian wavepacket, an expression valid only for a free particle corresponding to a system initialized at very large separation.

Total integral cross sections (ICSs) are calculated by summing over the values of reaction probabilities for all those J values including all the rovibrational states. The ICS at a total energy E is given by

$$\sigma_{v'j' \leftarrow vj}(E) = \frac{\pi}{\kappa^2_{vj}} \sum_{j'=0}^{j'_{max}} \sum_{v'=0}^{v'_{max}} \sum_{J=0}^{J_{max}} (2J+1) P^J_{v'j' \leftarrow vj}(E) \tag{37}$$

where $\kappa^2_{vj} = 2\mu_R(E - E_{vj})/\hbar^2$, μ_R is the reduced mass for the reactant channel, E_{vj} is the energy of the initial state, j'_{max} and v'_{max} are the highest open product rotational and vibrational states, respectively, J_{max} is the highest J value contributing in the considered energy range, and $P^J_{v'j' \leftarrow vj}(E)$ is the reaction probability.

Moreover, we introduce the partial cross section (PCS) defined as

$$\sigma^J_{v'j' \leftarrow vj}(E) = \frac{\pi}{\kappa^2_{vj}} \sum_{j'=0}^{j'_{max}} \sum_{v'=0}^{v'_{max}} (2J+1) P^J_{v'j' \leftarrow vj}(E) \tag{38}$$

and thus, the integral cross section can be expressed as

$$\sigma_{v'j' \leftarrow vj}(E) = \sum_{J=0}^{J_{max}} \sigma^J_{v'j' \leftarrow vj}(E) \tag{39}$$

IIA. The absorbing potential. Since, for any realistic scattering calculation, one cannot set up the boundary at infinity, the outgoing wave packet must be removed from the grid just after the projection but before reaching the grid boundary in order to avoid any unphysical reflection. This can be done by incorporating a negative imaginary potential $[-iV_{Im}(\rho)]$ at the last 20% grid points for the hyperradius at each θ and ϕ.

Thus, the total potential of the system becomes

$$V(\rho, \theta, \phi) = V_0(\rho, \theta, \phi) - iV_{Im}(\rho) \tag{40}$$

This absorbing potential is placed far away from the interaction region. The imaginary potential can be of arbitrary form, where the only requirement is that the scattering amplitudes should not depend on the type of function employed as absorbing potential. In our present calculation, we have employed a linear absorbing potential[82,95] of the following form:

$$V_{Im}(\rho) = \begin{cases} V_{max} \cdot (\rho - \rho_I), & \rho_I \leq \rho \\ 0, & \text{otherwise,} \end{cases}$$

where ρ_I is the starting point for such a potential. Numerical adjustment of the magnitude of V_{max} (see Table I) is done in such a way so that the reflection of the wave function from the boundary is minimum.

IIB. Propagation, projection, and computation details. The evaluation of the kinetic energy operator by employing the Fast Fourier Transformation (FFT)[96] method is the actual bottleneck for the propagation of the wave packet. The FFT algorithm efficiently scales the computational effort as $cN \log N$, where N denotes the total number of grid points on the ρ, θ, and ϕ coordinates. The iterative Lanczos reduction technique[97] is employed to carry out the time propagation of the wave packet. Such a technique is a short time propagator that can automatically control the recursion by monitoring the magnitude of last few vectors, and can accurately analyze the outgoing wave packet. After each time step of propagation, the transformation matrix constituted with the Lanczos recursion vectors is stored in the core memory to avoid repeated calculation for half of such vectors, as required for the next time step. Due to the following reasons, the CPU time requirement is very high: (a) The recursive calculation of the kinetic energy

DOI: 10.1021/acs.jpca.5b07718
J. Phys. Chem. A XXXX, XXX, XXX−XXX

Table I. Data for Initialization, Projection, and Absorbing Potential Discussed in the Text: $v = 0$, $j = 0$, and $J = 0, 1, ..., 25$

Grid size:	
N_ρ	256
N_θ	64
N_ϕ	128
(ρ_{min}, ρ_{max})/Å	(1.1, 10.0)
Translational wave packet:	
R_0/Å	5.50 (~6.56)[a]
σ/Å	0.20
k_0 (Å^{-1})	36.3523
Initial state:	
E_{vj} (eV)	0.2698
Propagation:	
Δt (10^{-16} s)	0.50
Magnitude of the five last Lanczos vectors[b]	10^{-8}–10^{-7}
Absorbing potential:	
V_{max}/eV	0.163
ρ_I (Å)	8.0
Range of the absorbing potential (Å)	8.0–10.0
Projection:	
R^* (Å)	4.75 (~5.85)[a]
vib. states	$v' = 0, ..., 10$
rot. states	$j' = 0, ..., 12$

[a]The values in the parentheses are the transformed values in ρ-space. [b]The vectors are normalized; that is, the total magnitude of all vectors is one.

operators by employing the iterative Lanczos propagation method is dependent on the number of grid points, which can be up to 2×10^6 ($256 \times 64 \times 128$). (b) As the basis functions (plane waves) do not vanish at $\theta = \pi/2$, the doubling of grid size in the θ domain (originally varying from 0 to $\pi/2$ in the hyperspherical coordinate system) is necessary to ensure that the basis functions do vanish at $\theta = 0$ and π, leading to a sine transformation (see Appendix C of ref 47). (c) CPU time increases wildly with the increase of the total angular momentum, in particular, due to the projection of the time-dependent wave packets on the various asymptotic states (v', j') for different orbital angular momenta (l'). However, the execution time has been reduced enormously by using a parallelization scheme for the propagation and projection of the wave packet. The Open Multi-Processing (OpenMP) parallelization is implemented for calculation of a set of K-component waves for a particular J on a specific PES. In fact, the elapsed time for parallel computation has been shown to have clear gain over the serial analogue (see the Appendix in ref 48). On the other hand, the calculation on different PESs has been carried out by employing Massage Passing Interface (MPI) parallelization. The MPI scheme can take care of the fact that dynamics on all the three states can be computed simultaneously by performing the calculation at different computer nodes, which eventually diminishes the execution time further.

III. RESULTS AND DISCUSSION

We carry out time-dependent 3D as well as coupled 3D wave packet $[\Phi^d_{K,I}(\rho, \theta, \phi)]$ dynamics in hyperspherical coordinates for the $D^+ + H_2$ ($v = 0$; $j = 0$) reaction employing the diabatic PES involving the three lowest singlet states ($1^1A'$, $2^1A'$, and $3^1A'$). Such a PES has been obtained from accurate *ab initio* data for the singlet H_3^+ system using the Double Many Body Expansion (DMBE)[69] method. The important features of the adiabatic PESs, such as well depth, exoergicity, etc., and also the avoided crossing between the first two states ($1^1A'$ and $2^1A'$) are shown in Figure 2 of the Supporting Information (SI) and Figure 1, respectively. Regarding its high accuracy, it is sufficient here to note that it reproduces the most accurate band origins[98] within 1 cm^{-1} or so. Reaction probabilities for noncharge transfer (RNCT) as well as charge transfer (RCT and NRCT) processes are evaluated for situations involving both zero and nonzero total angular momenta starting from $J = 0$ to 25. Indeed, we have included all the helicity quantum numbers (K) which depend upon the initial rotational state (j) of the diatom and total angular momentum (J) of the triatom. Various parameters involved in our dynamical calculations are depicted in Table I. For all calculations, a larger set of grid basis ($256 \times 64 \times 128$) for the ρ, θ, and ϕ coordinates is employed even though reaction probabilities appeared to be well converged with a smaller basis set ($128 \times 64 \times 128$). Moreover, since the interpolation of the wave packet on the ρ coordinate is done during the projection at a particular R (i.e., R^*), the dynamics carried out with a higher number of grid points on the ρ coordinate is preferred.

In Figure 2, we present total reaction probabilities for the RNCT process of the $D^+ + H_2$ ($v = 0$; $j = 0$) reaction at $J = 0$, 4, 8, 12, 16, 18, 20, 22, and 25 performed on the lowest three singlet states of the diabatic DMBE PES for H_3^+ ($1^1A'$, $2^1A'$, $3^1A'$). The calculated probabilities for zero total angular momentum are compared with Chu and Han's[87] diabatic results obtained by using the KBNN PES.[68] For $J = 0$, the obtained profile is found to oscillate around 0.6 over the calculated energy range, while Chu and Han results appear to fluctuate between 0.5 and 0.7 over the same collision energies. The substantial differences between the two profiles for $J = 0$ in terms of features as well as magnitudes are most likely due to the PESs used in the dynamics calculations. The magnitudes of reaction probabilities for the RNCT process are found to gradually decrease as J increases from 0 to 12 within the entire energy range, and then they tend to increase with J up to $J = 16$,

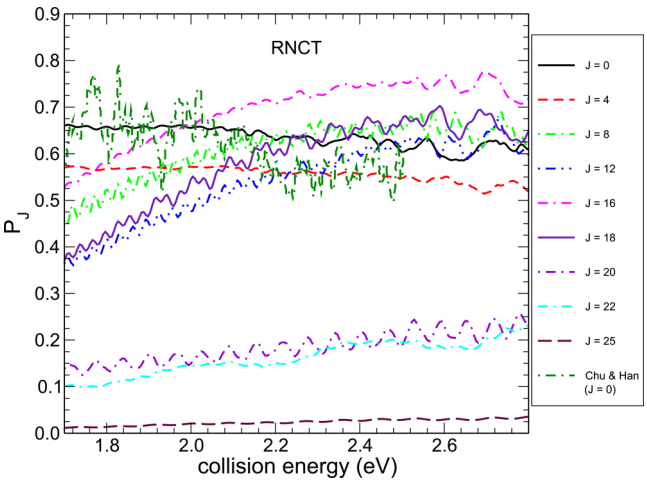

Figure 2. Total reaction probabilities, $P_{J=0}(E_{coll})$, as a function of collision energy for the reactive noncharge transfer (RNCT) process of the $D^+ + H_2(v = 0, j = 0)$ reaction with total angular momentum $J = 0$, 4, 8, 12, 16, 18, 20, 22, and 25. Also a comparison between the present result and the previous theoretical result[87] for the $J = 0$ case is shown.

DOI: 10.1021/acs.jpca.5b07718
J. Phys. Chem. A XXXX, XXX, XXX–XXX

particularly, in the lower collision energy regime, and, finally, to decrease at all energies beyond $J = 16$ to $J = 25$. On the other hand, the total reaction probabilities for the the RCT process of the same reaction are displayed in Figure 3. Although, for a

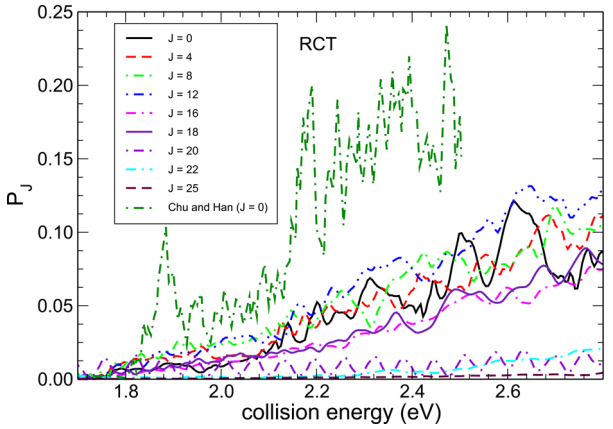

Figure 3. Same as Figure 2, but for the reactive charge transfer (RCT) process.

particular J, there is an overall increasing trend of the reaction probabilities as the collision energy increases, those probabilities generally decrease with the increment of J. The RCT profile shows a threshold collision energy (~1.8 eV) at $J = 0$, with such a threshold becoming larger for $J \neq 0$ due to the existence of a centrifugal barrier. Finally, Figure 4 depicts the

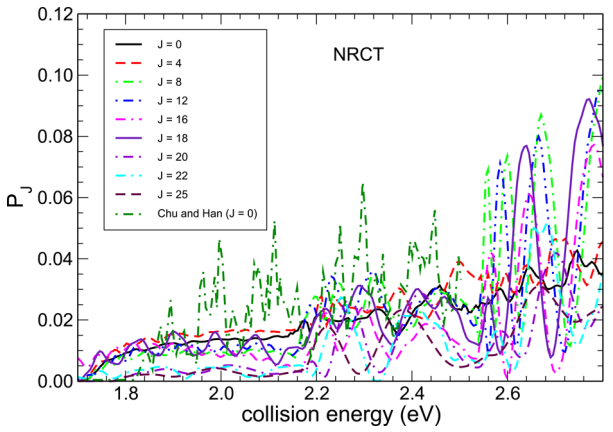

Figure 4. Same as Figure 2, but for nonreactive charge transfer (NRCT) process.

NRCT process, where the total reaction probabilities follow almost the same trend as in the RCT process. The threshold collision energy is quite evident from the profiles, which essentially appear to be the same as for RCT. Both in RCT and NRCT processes, the overall magnitudes of the reaction probability gradually tend to diminish as total angular momentum increases over the entire collision energy range, whereas, in the higher energy regime, the features are quite different due to prominent resonances. At this point, it is important to note that we have included all the K-component waves by employing the fully closed coupled (FCC) approach described elsewhere.[49] Since the approximate close coupled (ACC) approach[87] was shown to produce substantially different reaction probabilities, any approximation by considering a limited number of K-waves cannot be accurate enough. The differences observed with the previous theoretical results[87] may then be largely attributed to the different approaches (FCC vs ACC) used in solving the TDSE.

Figure 5 shows the convergence profiles of the total reaction probability for the RNCT process at five different collision

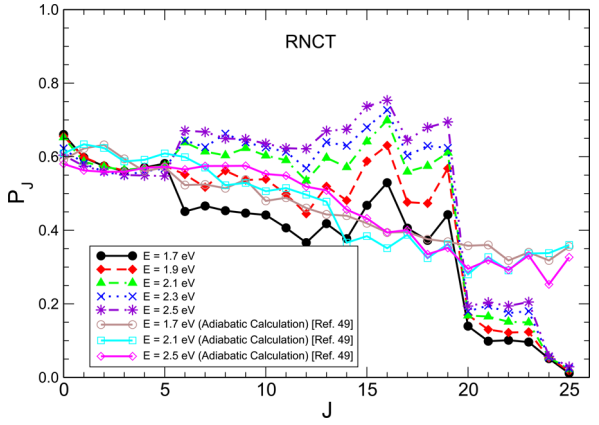

Figure 5. Convergence profiles of total reaction probability, P_J, at five different collision energies, namely, 1.7, 1.9, 2.1, 2.3, and 2.5 eV, for the RNCT process in the $D^+ + H_2$ ($v = 0$, $j = 0$) reaction. For comparison, the results of previous calculations[49] on the lowest adiabatic singlet surface ($1^1A'$) are also shown..

energies, namely, 1.7, 1.9, 2.1, 2.3, and 2.5 eV. At low collision energies (1.7 eV), the reaction probability attains a higher value for $J = 0$ and, then, gradually decreases up to $J = 12$ before it fluctuates around an average value up to $J = 16$, and, finally, decreases all along until $J = 25$. The trends for $E_{coll} = 1.9$, 2.1, 2.3, and 2.5 eV are almost similar to the one for $E_{coll} = 1.7$ eV except for little bit higher magnitudes from $J = 5$ onward. Also shown in the same plot are the profiles of reaction probabilities for the RNCT process obtained[49] from scattering calculations on the lowest adiabatic singlet state ($1^1A'$) of the DMBE PES. Note that, for a specific J, the calculated diabatic and adiabatic results display substantially different features as the collisional energy increases from 1.7 to 2.5 eV. On the other hand, when looking to the convergence profile for RCT probabilities in Figure 6, the situation appears to be somewhat different. At low collision energies (1.7 eV), the reaction probability is very close to zero for all J values, which reflects the threshold collision energy for opening channels due to nonadiabatic processes. Contrary to this, at high collision energies (1.9, 2.1, 2.3, and 2.5

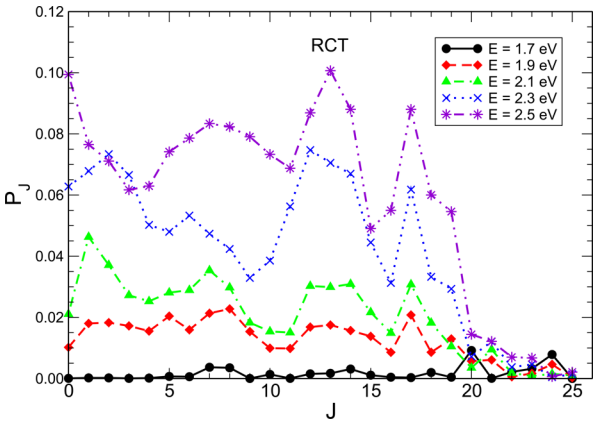

Figure 6. Same as Figure 5, but for the RCT process.

DOI: 10.1021/acs.jpca.5b07718
J. Phys. Chem. A XXXX, XXX, XXX−XXX

eV), the profiles have some peaks and deeps, which eventually fluctuate around some smaller value of the reaction probability up to J = 16 before those decay fast to small magnitudes from J = 18 to 25. For the NRCT process, the convergence plots are depicted in Figure 7. The small value of the reaction probability

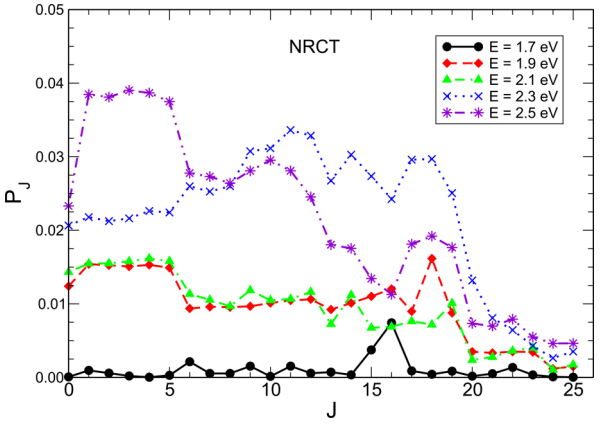

Figure 7. Same as Figure 5, but for the NRCT process.

at low energies (1.7 eV) provides here too clear evidence for the existence of a threshold energy, a scenario similar to the RCT case. Conversely, at high energies (1.9 and 2.1 eV), the magnitudes of the probabilities from J = 1 to J = 14 appear to be very close, but at higher energies (2.3 and 2.5 eV), those probabilities are widely different as a function of J. Such profiles fluctuate beyond J = 15 to J = 18 before finally decaying to small magnitudes from J = 19 to 25.

When the collision is performed considering the ground rovibrational initial state of H_2 (v = 0, j = 0) within the range of 1.7−2.5 eV initial collision energies for D^+, we have calculated and plotted the (2J+1)-weighted partial cross sections for the RNCT, RCT, and NRCT processes at five different collision energies (1.7, 1.9, 2.1, 2.3, and 2.5 eV). Such (2J+1)-weighted partial cross sections (often called opacity function) for the RNCT process are shown in Figure 8, where those functions increase gradually with J, reach a maximum around J = 19, and diminish to very small magnitude at J = 25. Also shown in the same figure are our previous adiabatic calculations.[49] Note that

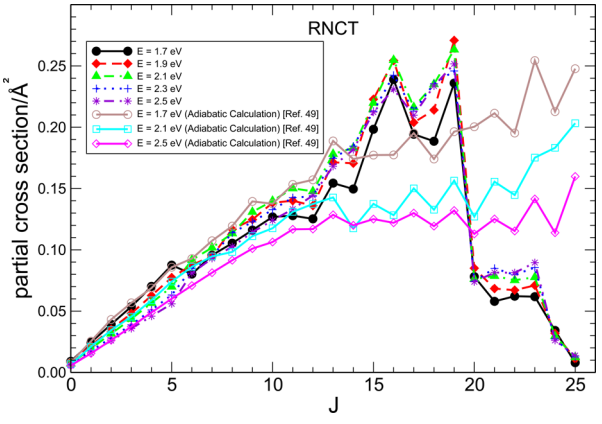

Figure 8. (2J+1)-weighted partial cross sections as a function of total angular momentum at five different collision energies, namely, 1.7, 1.9, 2.1, 2.3, and 2.5 eV, for the RNCT process in $D^+ + H_2$ (v = 0, j = 0). For comparison, the results of previous calculations[49] on the lowest adiabatic singlet surface ($1^1A'$) are also shown.

the RNCT partial cross sections calculated from the diabatic PESs show a distinct pattern when compared to adiabatic analogues as a function of J at various collisional energies. While the RNCT partial cross sections from the diabatic calculations increase with J up to a specific value and then saturate as the collisional increases from 1.7 to 2.5 eV, the same quantities from the adiabatic calculations decrease with kinetic energy for the same J. Thus, when the RNCT and RCT processes are simultaneously active at those collisional energies, the trend obtained from the diabatic calculations is to be expected rather than the adiabatic one. In the case of the RCT process (shown in Figure 9), the basic features of the curves are

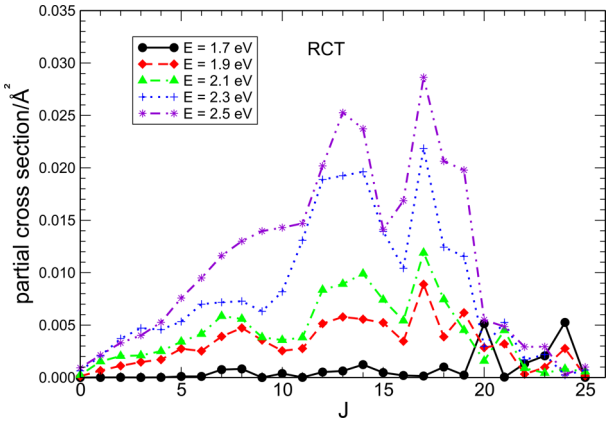

Figure 9. Same as Figure 8, but for the RCT process.

the same, but the relative magnitudes of the partial cross sections increase gradually with the increase of the collision energy. The maximum values are seen to be at different locations at five different energies. The opacity functions for the NRCT process have been displayed in Figure 10, where the trends are similar to that of the RCT case and the peak values become right shifted with the increase of collision energy.

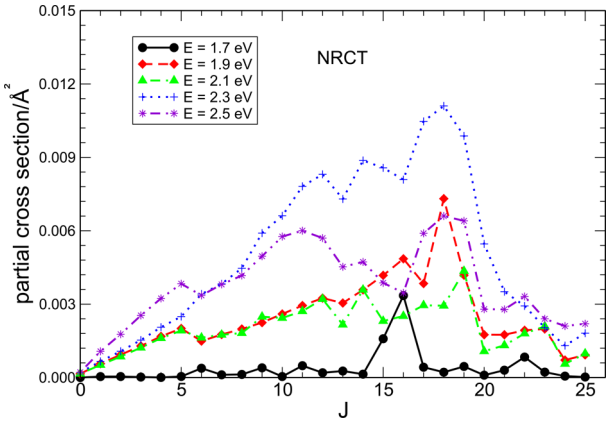

Figure 10. Same as Figure 8, but for the NRCT process.

The total integral cross sections for the RNCT process are obtained by summing over those opacity functions of all final rovibrational states and are presented in Figure 11. In the same plot, previous theoretical results[81,87] performed on both the DMBE[69] and KBNN[68] PESs along with the experimental results[67] and our previous adiabatic calculation[49] are also given for comparison. It is seen from this figure that our diabatic results are in close agreement with the experimental results as

DOI: 10.1021/acs.jpca.5b07718
J. Phys. Chem. A XXXX, XXX, XXX−XXX

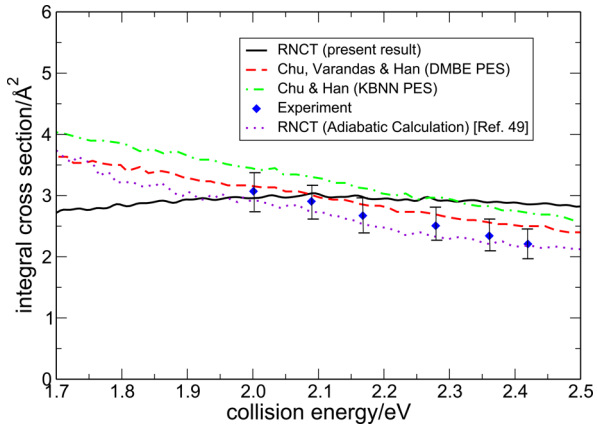

Figure 11. Total integral cross section of the $D^+ + H_2$ ($v = 0$, $j = 0$) reaction for the RNCT process by implicating the FCC formalism along with the comparison with previous calculations[49,81,87] and experimental measurements.[67] The black curve indicates the present results, whereas the red, green, and violet curves refer to other theoretical calculations employing the DMBE and KBNN PESs, respectively.

well as the calculated ones[81] performed on the DMBE PES. In the collision energy range of 1.7−2.3 eV, the magnitudes of the integral cross sections fall within the experimental error bars, whereas the results obtained by Chu and Han[87] on the KBNN PES lie somewhat away from the experimental findings. However, the other calculations[81] employing the ACC approach are in good agreement with the experimental results, which gives an indication about the crucial contribution of the PES (KBNN and DMBE) to the cross section. Since both previous calculations used the ACC approach, it is expected that few *K*-waves cannot lead to accurate numbers while solving the TDSE as illustrated elsewhere.[49] At higher collision energy (2.3−2.5 eV), our results deviate from the experimental ones, which may be due to the shortcomings in the PES employed for the calculation. On the other hand, in Figure 12, we have

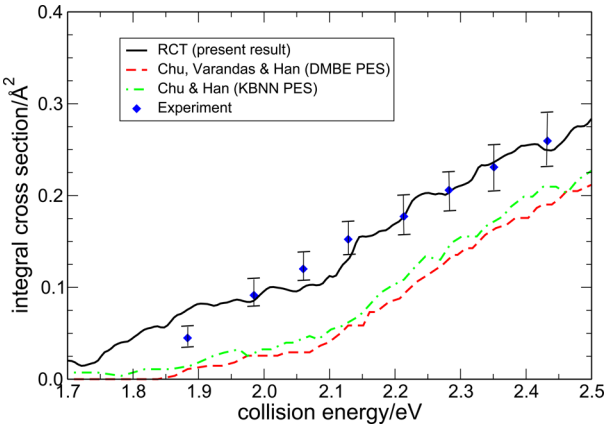

Figure 12. Same as Figure 11, but for the RCT process.

displayed total integral cross sections for reactive charge transfer (RCT) processes as a function of the collision energy along with other theoretical calculations[81,87] and experimental results.[67] Clearly, the present calculations agree quite well with the experimental values, while the others[81,87] lie somewhat outside the error bars. Unlike RNCT, the RCT profile gradually increases with collision energy, with the small magnitude of the cross section at low collision energies indicating a threshold for the nonadiabatic processes. While analyzing carefully the figures for the cross sections in the RNCT (Figure 11) and RCT (Figure 12) processes, it appears that not only a small increase of cross section in RNCT is observed around 2.1 eV but also the cross section for the RCT process shows a slight dip around the same energy. Indeed, similar features are present for the RNCT and RCT processes in the calculated partial cross sections as a function of J for different collisional energies. In other words, partial cross sections for the RNCT process increase with the collisional energy from 1.7 to 2.1 eV and then either saturate or slightly decrease at 2.3 as well as 2.5 eV for any specific J (see Figure 8) whereas, in the case of the RCT process, such partial cross sections increase with lower rate up to 2.1 eV and then steeply increase from 2.3 to 2.5 eV (see Figure 9). Such a feature is also observed in the reaction probability profiles, namely for a particular J (say, $J = 15$), with the RNCT probabilities manifesting a substantial increase from 1.7 to 2.1 eV and then showing only a small enhancement for 2.3 and 2.5 eV (see Figure 5), which is more or less opposite to the trend displayed by the RCT process (see Figure 6). As a result, the competition between the RNCT and RCT processes becomes prominent at about 2.1 eV, where the RNCT and RCT cross sections increase with collisional energy up to 2.1 eV, although beyond this energy RCT dominates over RNCT. Of course, the validity of the present result and its interpretation may demand even more accurate *ab initio* diabatic PESs and, indeed, accurate experimental results. Finally, we have presented the integral cross section for the NRCT process as a function of collision energy in Figure 13.

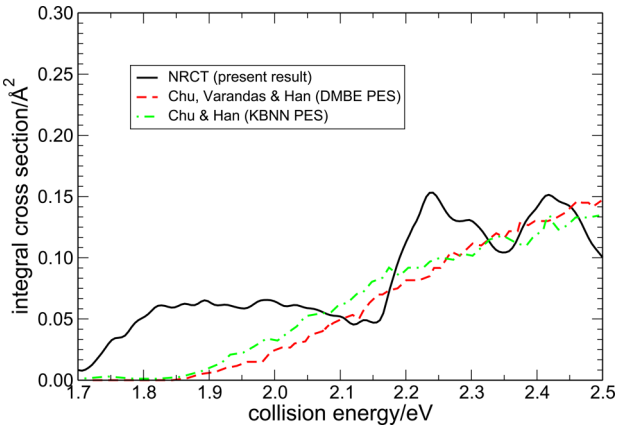

Figure 13. Same as Figure 11, but for the NRCT process.

Since the experimental data for the NRCT process is not yet available, we have shown comparisons only with the previous theoretical results.[81,87] The present profile for the NRCT process does not show good agreement with the other calculations.[81,87] Indeed, the cross sections for RCT and NRCT processes increase with collision energy, and their magnitudes are small at low collision energies.

IV. SUMMARY

We have explored our methodology by using the coupled 3D wave packet method in hyperspherical coordinates (ρ, θ, ϕ) for the RNCT, RCT, and NRCT competing processes of the $D^+ + H_2$ reaction. The diabatic quantum dynamics calculation uses the grid representation aprroach in hyperspherical coordinates, where a basis set (Wigner **D** matrix) expansion is used to

DOI: 10.1021/acs.jpca.5b07718
J. Phys. Chem. A XXXX, XXX, XXX−XXX

quantize the triatomic plane of rotation. Our methodology and code are advantageous for two reasons: (a) requirement of a smaller number of basis functions for the quantization of rotation of the triatomic plane than the number of grid points for the representation of any other internal coordinates (ρ, θ, ϕ); (b) efficient parallellization (mixed OpenMP-MPI) of the algorithm with nearly the same execution time for increasing J values and some reduction of the execution time for different PESs. Although the major time-consuming part of the code is due to FFT evaluation of the kinetic energy terms, a substantial reduction of the elapsed time is obtained via implementation of parallel FFT algorithms through vectorization of the grid.

In the present work, we have performed coupled 3D time-dependent wave packet calculations in hyperspherical coordinates for treating evenhandedly all three competing processes, namely, RNCT, RCT, and NRCT, of the $D^+ + H_2(v = 0, j = 0)$ reaction, with the diabatic potential energy surfaces for the lowest three singlet states ($1^1A'$, $2^1A'$, and $3^1A'$) modeled by the accuate DMBE PES.[69] Our major focus has been on investigating the nonadiabatic effects which are known to contribute at higher energies beyond ~1.8 eV. All K-waves have been utilized for each J, as these were shown to contribute significantly[49] over the entire energy range. The total reaction probabilities for $J = 0$ are in good agreement with the previous results of Chu and Han at the lower collision energy range, whereas, at the higher energy regime, the magnitudes of the probabilities deviate from each other, most probably due to the adaptation of different PES (DMBE[69] vs KBNN[68]) and implementation of different dynamical approaches (ACC and FCC).[49] From our calculations, it appears that, for the ground rovibrational initial state of H_2, the RNCT process is the dominant one, as it exhibits the largest cross section. As the collision energy increases, two charge transfer processes (RCT and NRCT) grow with increasing contribution, whereas in the case of RNCT, it is the reverse. Whenever possible, a comparison with the experimental measurements has been made. Total integral cross sections for the RNCT process show good agreement with experiment over all studied collision energies, while the reactive charge transfer process matches well the corresponding experimental findings.

■ ASSOCIATED CONTENT

Supporting Information

The Supporting Information is available free of charge on the ACS Publications website at DOI: 10.1021/acs.jpca.5b07718.

Figures describing the positions of the atoms in space-fixed and body-fixed coordinate systems, schematic representation of the potential energy curves (PECs), and tables corresponding to the reaction probabilities for various J values (PDF)

■ AUTHOR INFORMATION

Corresponding Authors

*Fax: +91-33-2473 2805. E-mail: pcsa@iacs.res.in.

*E-mail: varandas@uc.pt.

Present Address

§(R.S.) St. Xavier's College, 30 Mother Teresa Sarani, Kolkata-700016, West Bengal, India.

Notes

The authors declare no competing financial interest.

■ ACKNOWLEDGMENTS

S.A. thanks IACS for access to the CRAY computing facility. S.G. acknowledges CSIR, India, for a research fellowship. R.S. and A.J.C.V. acknowledge the financial support of FEDER through "Programa Operacional Factores de Competitividade-COMPETE" (COMPETE/FEDER-FCOMP-01-0124-FEDER-008517), and national funds under the auspices of Fundação para a Ciência e a Tecnologia contracts PTDC/CEQ-COM/3249/2012, and PTDC/AAG-MAA/4657/2012), Portugal, whose support to the Coimbra Chemistry Centre through the project PEst-OE/QUI/UI0313/2014 is also acknowledged.

■ REFERENCES

(1) Diestler, D. J.; McKoy, V. Quantum-Mechanical Treatment of Inelastic Collisions. II. Exchange Reactions. *J. Chem. Phys.* **1968**, *48*, 2951−2959.

(2) Truhlar, D. J.; Kuppermann, A. Quantum Mechanics of the H + H_2 Reaction: Exact Scattering Probabilities for Collinear Collisions. *J. Chem. Phys.* **1970**, *52*, 3841−3843.

(3) Miller, G.; Light, J. C. Quantum Calculations of Collinear Reactive Triatomic Systems. II. Theory. *J. Chem. Phys.* **1971**, *54*, 1635−1642.

(4) McCullough, E. A.; Wyatt, R. E. Dynamics of the Collinear H + H_2 Reaction. I. Probability Density and Flux. *J. Chem. Phys.* **1971**, *54*, 3578−3591.

(5) Schatz, G. C.; Bowman, J.; Kuppermann, A. Large Quantum Effects in the Collinear F + H_2 →FH + H Reaction. *J. Chem. Phys.* **1973**, *58*, 4023−4025.

(6) Kouri, D. J.; Baer, M. Collinear Quantum Mechanical Calculations of the He + H_2^+ Proton Transfer Reaction. *Chem. Phys. Lett.* **1974**, *24*, 37−40.

(7) Persky, A.; Baer, M. Exact Quantum Mechanical Study of Kinetic Effects in the Collinear Reaction Cl + H_2 →HCl + H. The H_2/D_2 and the H_2/T_2 Isotope Effects. *J. Chem. Phys.* **1974**, *60*, 133−136.

(8) Schatz, G. C.; Bowman, J.; Kuppermann, A. Exact Quantum, Quasiclassical, and Semiclassiacal Reaction Probabilities for the Collinear F + H_2→FH + H Reaction. *J. Chem. Phys.* **1975**, *63*, 674−684.

(9) Kuppermann, A.; Schatz, G. C.; Baer, M. Quantum Mechanical Reactive Scattering for Planar Atom Plus Diatom Systems. I. Theory. *J. Chem. Phys.* **1976**, *65*, 4596−4623.

(10) Webster, F.; Light, J. C. Atom-Diatom Reactive Scattering. I. Quantum Theory. *J. Chem. Phys.* **1989**, *90*, 265−299.

(11) Mishra, M.; Linderberg, J.; Ohrn, Y. Characterization of Adiabatic States in Triatomic Collisions. *Chem. Phys. Lett.* **1984**, *111*, 439−444.

(12) Hipes, P. G.; Kuppermann, A. Lifetime Analysis of High-Energy Resonances in Three-Dimensional Reactive Scattering. *Chem. Phys. Lett.* **1987**, *133*, 1−7.

(13) Pack, R. T.; Parker, G. A. Quantum Reactive Scattering in Three Dimensions Using Hyperspherical (APH) Coordinates. Theory. *J. Chem. Phys.* **1987**, *87*, 3888−3921.

(14) Schatz, G. C. Quantum Reactive Scattering Using Hyperspherical Coordinates: Results for H + H_2 and Cl + HCl. *Chem. Phys. Lett.* **1988**, *150*, 92−98.

(15) Launay, J. M.; Lepetit, B. Three-Dimensional Quantum Study of the Reaction F + FH(vj) →HF($v'j'$) + H in Hyperspherical Coordinates. *Chem. Phys. Lett.* **1988**, *144*, 346−352.

(16) Zhang, J. Z. H.; Miller, W. H. New Method for Quantum Reactive Scattering, with Applications to the 3-D H + H_2 Reaction. *Chem. Phys. Lett.* **1987**, *140*, 329−337.

(17) Zhang, J. Z. H.; Miller, W. H. Quantum Reactive Scattering via the S-Matrix Version of the Kohn Variational Principle: Integral Cross Sections for H + H_2 ($v_1 = j_1 = 0$) →H_2 ($v_2 = 1$, $j_2 = 1,3$) + H in the Energy Range E_{total} = 0.9−1.4 eV. *Chem. Phys. Lett.* **1988**, *153*, 465−470.

DOI: 10.1021/acs.jpca.5b07718
J. Phys. Chem. A XXXX, XXX, XXX−XXX

(18) Zhang, J. Z. H.; Miller, W. H. Quantum Reactive Scattering via the S-Matrix Version of the Kohn Variational Principle: Differential and Integral Cross Sections for D + H_2 →HD + H. *J. Chem. Phys.* **1989**, *91*, 1528−1547.
(19) Haug, K.; Schwenke, D. W.; Shima, Y.; Truhlar, D. G.; Zhang, J. Z. H.; Kouri, D. K. L^2 Solution of the Quantum Mechanical Reactive Scattering Problem. The Threshold Energy for $D + H_2(v = 1)$ →HD + H. *J. Phys. Chem.* **1986**, *90*, 6757−6759.
(20) Mladenovic, M.; Zhao, M.; Truhlar, D. G.; Schwenke, D. W.; Sun, Y.; Kouri, D. J. Converged Quantum Mechanical Calculation of the Product Vibration-Roatation State Distribution of the H + p-H_2 Reaction. *J. Phys. Chem.* **1988**, *92*, 7035−7038.
(21) Lee, Y. T. *Chem. Scr.* **1987**, *27*, 215.
(22) Lee, Y. T. Molecular Beam Studies of Elementary Chemical Processes. *Science* **1987**, *236*, 793.
(23) Kliner, D. A. V.; Adelman, D. E.; Zare, R. N. Comparison of Experimental and Theoretical Integral Cross Sections for D + H_2(v = 1, j = 1) →HD(v' = 1, j = l) + H. *J. Chem. Phys.* **1991**, *95*, 1648.
(24) Casavecchia, P. Chemical Reaction Dynamics with Molecular Beams. *Rep. Prog. Phys.* **2000**, *63*, 355−414.
(25) Liu, X.; Lin, J. J.; Harich, S. A.; Schatz, G. C.; Yang, X. A Quantum State-Resolved Insertion Reaction: $O(^1D) + H_2(J = 0) \rightarrow OH(^2\Pi,v,N) + H(^2S)$. *Science* **2000**, *289*, 1536−1538.
(26) Dobbyn, A. J.; McCabe, P.; Connor, J. N. L.; Castillo, J. F. Nearside-Farside Analysis of State-Selected Differential Cross Sections for Reactive Molecular Collisions. *Phys. Chem. Chem. Phys.* **1999**, *1*, 1115−1124.
(27) Kendrick, B. K. Geometric Phase Effects in the H + D_2 →HD + D Reaction. *J. Chem. Phys.* **2000**, *112*, 5679−5704.
(28) Sokolovski, D.; Castillo, J. F. Differential Cross Sections and Regge Trajectories for the F + H_2 →HF + H Reaction. *Phys. Chem. Chem. Phys.* **2000**, *2*, 507−512.
(29) Meijer, A. J. H. M.; Goldfield, E. M. Time-Dependent Quantum Mechanical Calculations on H + O_2 for Total Angular Momentum J > 0 II: On the Importance of Coriolis Coupling. *J. Chem. Phys.* **1999**, *110*, 870−880.
(30) Zhang, D. H.; Lee, S. Y.; Baer, M. Quantum Mechanical Integral Cross Sections and Rate Constants for the F + HD Reactions. *J. Chem. Phys.* **2000**, *112*, 9802−9809.
(31) Judson, R. S.; Kouri, D. J.; Neuhauser, D.; Baer, M. Time-Dependent Wave-Packet Method for the Complete Determination of S-Matrix Elements for Reactive Molecular Collisions in Three Dimensions. *Phys. Rev. A: At., Mol., Opt. Phys.* **1990**, *42*, 351−366.
(32) Gogtas, F.; Balint-Kurti, G. G.; Offer, A. R. Quantum Mechanical Three-Dimensional Wavepacket Study of the Li + HF →LiF + H Reaction. *J. Chem. Phys.* **1996**, *104*, 7927−7939.
(33) Zhu, W.; Peng, T.; Zhang, J. Z. H. Reactant-Product Decoupling Method for State-to-State Reactive Scattering: A Case Study for 3D H + H_2 Exchange Reaction (J = 0). *J. Chem. Phys.* **1997**, *106*, 1742−1748.
(34) Althorpe, S. C.; Kouri, D. J.; Hoffmann, D. K. A Chebyshev Method for Calculating State-to-State Reaction Probabilities from Time-Independent Wavepacket Reactant-Product Decoupling Equations. *J. Chem. Phys.* **1997**, *106*, 7629−7636.
(35) Althorpe, S. C.; Kouri, D. J.; Hoffmann, D. K. State-to-State Reaction Probabilities from the Time-Independent Wavepacket Reactant-Product Decoupling Equations: Application to the Three-Dimensional H + H_2 Reaction (for J = 0. *Chem. Phys. Lett.* **1997**, *275*, 173−180.
(36) Althorpe, S. C.; Kouri, D. J.; Hoffmann, D. K. Application of the Time-Independent Wave Packet Reactant-Product Decoupling Method to the (J = 0) Li + HF Reaction. *J. Phys. Chem. A* **1998**, *102*, 9494−9499.
(37) Juanes-Marcos, J. C.; Althorpe, S. C. On the Role of Conical Intersection in H + H_2 Reactive Scattering. *Chem. Phys. Lett.* **2003**, *381*, 743−750.
(38) Althorpe, S. C. Quantum Scattering with Energy-Filtered Plane Wave Packets: Visualizing the F + HD "Ridge" Mechanism. *J. Phys. Chem. A* **2003**, *107*, 7152−7160.
(39) Althorpe, S. C. Plane Wave Packet Formulation of Atom-Plus-Diatom Quantum Reactive Scattering. *J. Chem. Phys.* **2004**, *121*, 1175−1186.
(40) Juanes-Marcos, J. C.; Varandas, A. J. C.; Althorpe, S. C. Geometric Phase Effects in Resonance-Mediated Scattering: H + H_2^+ on its Lowest Triplet Electronic State. *J. Chem. Phys.* **2008**, *128*, 211101/1−5.
(41) Gao, H.; Sneha, M.; Bouakline, F.; Althorpe, S. C.; Zare, R. N. Dierential Cross Sections for the H + D_2 →HD(v' = 3, j' = 4−10) + D Reaction above the Conical Intersection. *J. Phys. Chem. A* **2015**, DOI: 10.1021/acs.jpca.5b04573.
(42) Gray, S. K.; Balint-Kurti, G. G. Quantum Dynamics with Real Wave Packets, Including Application to Three-Dimensional (J = 0) D + H_2 →HD + H. *J. Chem. Phys.* **1998**, *108*, 950−962.
(43) Lin, S. Y.; Guo, H. Quantum State-to-State Cross Sections for Atom-Diatom Reactions: A Chebyshev Real Wave-Packet Approach. *Phys. Rev. A: At., Mol., Opt. Phys.* **2006**, *74*, 022703/1−8.
(44) Gomez-Carrasco, S.; Roncero, O. Coordinate Transformation Methods to Calculate State-to-State Reaction Probabilities with Wave Packet Treatments. *J. Chem. Phys.* **2006**, *125*, 054102/1−14.
(45) Sun, Z.; Lin, X.; Lee, S.-Y.; Zhang, D. H. A Reactant-Coordinate-Based Time-Dependent Wave Packet Method for Triatomic State-to-State Reaction Dynamics: Application to the H + O_2 Reaction. *J. Phys. Chem. A* **2009**, *113*, 4145−4154.
(46) Sun, Z.; Guo, H.; Zhang, D. H. Extraction of State-to-State Reactive Scattering Attributes from Wave Packet in Reactant Jacobi Coordinates. *J. Chem. Phys.* **2010**, *132*, 084112/1−11.
(47) Zhang, P. Y.; Han, K. L. Adiabatic/Nonadiabatic State-to-State Reactive Scattering Dynamics Implemented on Graphics Processing Units. *J. Phys. Chem. A* **2013**, *117*, 8512−8518.
(48) Adhikari, S.; Varandas, A. J. C. The Coupled 3D Wave Packet Approach for Triatomic Reactive Scattering in Hyperspherical Coordinates. *Comput. Phys. Commun.* **2013**, *184*, 270−283.
(49) Sahoo, T.; Ghosh, S.; Adhikari, S.; Sharma, R.; Varandas, A. J. C. Coupled 3D Time-Dependent Wave-Packet Approach in Hyperspherical Coordinates: Application to the Adiabatic Singlet State ($1^1A'$) D^+ + H_2 Reaction. *J. Phys. Chem. A* **2014**, *118*, 4837−4850.
(50) Sahoo, T.; Ghosh, S.; Adhikari, S.; Sharma, R.; Varandas, A. J. C. Low Temperature D^+ + H_2 Reaction: A Time-Dependent Coupled Wave-Packet Study in Hyperspherical Coordinates. *J. Chem. Phys.* **2015**, *142*, 024304/1−9.
(51) Wu, Y. S. M.; Cuccaro, S. A.; Hipes, P. G.; Kuppermann, A. Quantum Mechanical Reactive Scattering Using a High-Performance Distributed-Memory Parallel Computer. *Chem. Phys. Lett.* **1990**, *168*, 429−440.
(52) Kress, J. D.; Pack, R. T.; Parker, G. A. Accurate Three-Dimensional Quantum Scattering Calculations for F + H_2 →HF + H with Total Angular Momentum J = 1. *Chem. Phys. Lett.* **1990**, *170*, 306−310.
(53) Launay, J. M.; Dourneuf, M. L. Quantum-Mechanical Calculations of Intergral Cross Sections for the Reaction F + H_2(v = 0, j = 0) →FH($v'j'$) + H by the Hyperspherical Method. *Chem. Phys. Lett.* **1990**, *169*, 473−481.
(54) Lepetit; Kuppermann, A. Numerical Study of the Geometrical Phase in the H + H_2 Reaction. *Chem. Phys. Lett.* **1990**, *166*, 581−588.
(55) Wu, Y.-S. M.; Kuppermann, A.; Leptit, B. Theoretical Calculation of Experimentally Observable Consequences of the Geometrical Phase on Chemical Reaction Cross Section. *Chem. Phys. Lett.* **1991**, *186*, 319−328.
(56) Castillo, J. F.; Manolopoulos, D. E. Quantum Mechanical Angular Distributions for the F + HD Reaction. *Faraday Discuss.* **1998**, *110*, 119−138.
(57) de Miranda, M. P.; Clary, D. C.; Castillo, J. F.; Manolopoulos, D. E. Using Quantum Rotational Polarization Momentsto Describe the Sterodynamics of the H + D_2(v = 0, j = 0) →HD(v', j') Reaction. *J. Chem. Phys.* **1998**, *108*, 3142−3153.
(58) Skouteris, D.; Manolopoulos, D. E.; Bian, W.; Werner, W. J.; Lai, L. H.; Liu, K. van der Waals Interactions in the Cl + HD Reaction. *Science* **1999**, *286*, 1713−1716.

DOI: 10.1021/acs.jpca.5b07718
J. Phys. Chem. A XXXX, XXX, XXX−XXX

(59) Honvault, P.; Launay, J. M. A Quantum-Mechanical Study of the Dynamics of the N(^{2}D) + H_2 →NH + H Reaction. *J. Chem. Phys.* **1999**, *111*, 6665−6667.
(60) Huarte-Larranaga, F.; Gimenez, X.; Lucas, J. M.; Aguilar, A.; Launay, J. M. Exact Quantum 3D Cross Sections for the Ne + H_2^+ → NeH^+ + H Reaction by the Hyperspherical Method. Comparison with Approximate Quantum Mechanical and Classical Results. *Phys. Chem. Chem. Phys.* **1999**, *1*, 1125−1132.
(61) Lagana, A.; Bolloni, A.; Crocchianti, S.; Parker, G. A. On the Effect of Increasing Total Angular Momentum on Li + HF Reactivity. *Chem. Phys. Lett.* **2000**, *324*, 466−474.
(62) Billing, G. D.; Markovic, N. Apparatus for Coupled 3D Wave-Packet Solution of Reactive Scattering Problem in Hyperspherical Coordinates. *J. Chem. Phys.* **1993**, *99*, 2674−2681.
(63) Markovic, N.; Billing, G. D. The Coupled Three-Dimensional Wave Packet Approach to Reactive Scattering. *J. Chem. Phys.* **1994**, *100*, 1085−1093.
(64) Crawford, J.; Parker, G. A. State-to-State Three-Atom Time-Dependent Reactive Scattering in Hyperspherical Coordinates. *J. Chem. Phys.* **2013**, *138*, 054313/1−12.
(65) Fehsenfeld, F. C.; Dunkin, D. B.; Ferguson, E. E.; Albritton, D. L. Measurement of the Rate Constant for the Reaction D^++H_2→DH +H^+. *Astrophys. J.* **1973**, *183*, L25−L26.
(66) Gerlich, D. Inhomogeneous rf Fields: A Versatile Tool for the Study of Processes with Slow Ions. *Adv. Chem. Phys.* **1992**, *82*, 1−176.
(67) Schlier, C.; Nowotny, U.; Teloy, E. Proton-Hydrogen Collision: Trajectory Surface Hopping Calculations and New Measurements. *Chem. Phys.* **1987**, *111*, 401−408.
(68) Kamisaka, A.; Bian, W.; Nobusada, K.; Nakamura, H. Accurate Quantum Dynamics of Electronically Nonadiabatic Chemical Reactions in the DH_2^+ System. *J. Chem. Phys.* **2002**, *116*, 654−665.
(69) Viegas, L. P.; Alijah, A.; Varandas, A. J. C. Accurate *ab initio* Based Multisheeted Double Many-Body Expansion Potential Energy Surface for the Three Lowest Electronic Singlet States of H_3^+. *J. Chem. Phys.* **2007**, *126*, 074309/1−9.
(70) Mukherjee, S.; Mukhopadhyay, D.; Adhikari, S. Conical Intersections and Diabatic Potential Energy Surfaces for the Three Lowest Electronic Singlet States of H_3^+. *J. Chem. Phys.* **2014**, *141*, 204306/1−13.
(71) Ochs, G.; Teloy, E. Integral Cross Sections for Reactions of H^+ with D_2; New Measurements. *J. Chem. Phys.* **1974**, *61*, 4930−4931.
(72) Fehsenfeld, F. C.; Albritton, D. L.; Bush, Y. A.; Fournier, P. G.; Govers, T. R.; Fournier, J. Ion-Atom Interchange Reactions Using Isotopic Species. *J. Chem. Phys.* **1974**, *61*, 2150−2155.
(73) Villinger, H.; Henchman, M. J.; Lindinger, W. Drift Tube Investigation of the Reactions H^+ + D_2 →HD + D^+ and D^+ + H_2 → HD + H^+ in the Relative Energy Range 0.04−0.3 eV. *J. Chem. Phys.* **1982**, *76*, 1590−1591.
(74) Henchman, M. J.; Adams, N. G.; Smith, D. The Isotope Exchange Reactions H^+ + D_2 →HD + D^+ and D^+ + H_2 →HD + H^+ in the Temperature Range 200−300 K. *J. Chem. Phys.* **1981**, *75*, 1201−1206.
(75) Preston, K.; Tully, J. C. Effect of Surface Crossing in Chemical Reactions: The H_3^+ System. *J. Chem. Phys.* **1971**, *54*, 4297−4304.
(76) Ushakov, V. G.; Nobusada, K.; Osherov, V. I. Electronically Nonadiabatic Transitions in a Collinear H_2 + H^+ System: Quantum Mechanical Understanding and Comparison with a Trajectory Surface Hopping Method. *Phys. Chem. Chem. Phys.* **2001**, *3*, 63−69.
(77) Ichihara, A.; Yokoyama, K. *Ab initio* Potential Energy Surfaces for the Two Lowest $^1A'$ States of H_3^+. *J. Chem. Phys.* **1995**, *103*, 2109−2112.
(78) Aguado, A.; Roncero, O.; Tablero, C.; Sanz, C.; Paniagua, M. Global Potential Energy Surfaces for the H_3^+ System. Analytical Representation of the Adiabatic Ground-State $1^1A'$ Potential. *J. Chem. Phys.* **2000**, *112*, 1240−1254.
(79) Velilla, L.; Leptit, B.; Aguado, A.; Beswick, A.; Paniagua, M. The H_3^+ Rovibrational Spectrum Revisited with a Global Electronic Potential Energy Surface. *J. Chem. Phys.* **2008**, *129*, 084307/1−11.
(80) Sarkar, B.; Adhikari, S. Extended Born-Oppenheimer Equation for a Three-State System. *J. Chem. Phys.* **2006**, *124*, 074101/1−18.
(81) Chu, T. S.; Varandas, A. J. C.; Han, K. L. Nonadiabatic Effects in D^+ + H_2 and H^+ + D_2. *Chem. Phys. Lett.* **2009**, *471*, 222−228.
(82) Markovic, N.; Billing, G. D. Wave Packet Calculations on Ion−Molecule Reactions. *Chem. Phys.* **1995**, *191*, 247−260.
(83) Takayanagi, T.; Kurosaki, Y.; Ichihara, A. Three-Dimensional Quantum Reactive Calculations for the Nonadiabatic (D + H_2)$^+$ Reaction System. *J. Chem. Phys.* **2000**, *112*, 2615−2622.
(84) Li, B.; Han, K. L. The Three-Dimensional Nonadiabatic Dynamics Calculation of DH_2^+ and HD_2^+ Systems by Using the Trajectory Surface Hopping Method Based on the Zhu-Nakamura Theory. *J. Chem. Phys.* **2008**, *128*, 114116/1−7.
(85) Ichihara, A.; Shirai, T.; Yokoyama, K. A Study on Ion−Molecule Reactions in the H_3^+ System with the Trajectory-Surface-Hopping Model. *J. Chem. Phys.* **1996**, *105*, 1857−1861.
(86) Last, I.; Gilibert, M.; Baer, M. A Three-Dimensional Quantum Mechanical Study of the H + H_2^+ →H_2 + H^+ System: Competition between Chemical Exchange and Inelastic Processes. *J. Chem. Phys.* **1997**, *107*, 1451−1459.
(87) Chu, T. S.; Han, K. L. Nonadiabatic Time-Dependent Wave Packet Study of the D^+ + H_2 Reaction System. *J. Phys. Chem. A* **2005**, *109*, 2050−2056.
(88) Lu, R. F.; Chu, T. S.; Han, K. L. Quantum Wave Packet Study of the H^+ + D_2 Reaction on Diabatic Potential Energy Surfaces. *J. Phys. Chem. A* **2005**, *109*, 6683−6688.
(89) Chu, T. S.; Han, K. L. Effect of Coriolis Coupling in Chemical Reaction Dynamics. *Phys. Chem. Chem. Phys.* **2008**, *10*, 2431−2441.
(90) Chu, T.; Han, K. L. Coriolis Coupling Effect in Molecular Reaction Dynamics. *Annu. Rep. Prog. Chem., Sect. C: Phys. Chem.* **2012**, *108*, 10−33.
(91) Gonzalez-Lezana, T.; Honvault, P. The H^+ + H_2 Reaction. *Int. Rev. Phys. Chem.* **2014**, *33*, 371−395.
(92) Chu, T. S.; Zhang, Y.; Han, K. L. The Time-Dependent Quantum Wave Packet Approach to the Electronically Nonadiabatic Processes in Chemical Reactions. *Int. Rev. Phys. Chem.* **2006**, *25*, 201−235.
(93) Arthurs, A. M.; Dalgarno, A. The Theory of Scattering by a Rigid Rotator. *Proc. R. Soc. London, Ser. A* **1960**, *256*, 540−551.
(94) Johnson, B. R. The Quantum Dynamics of Three Particles in Hyperspherical Coordinates. *J. Chem. Phys.* **1983**, *79*, 1916−1925.
(95) Neuhasuer, D.; Baer, M. The Time-Dependent Schrödinger Equation: Application of Absorbing Boundary Conditions. *J. Chem. Phys.* **1989**, *90*, 4351−4355.
(96) Kosloff, D.; Kosloff, R. A Fourier Method Solution for the Time Dependent Schrödinger Equation as a Tool in Molecular Dynamics. *J. Comput. Phys.* **1983**, *52*, 35−53.
(97) Park, T. J.; Light, J. C. Unitary Quantum Time Evolution by Iterative Lanczos Reduction. *J. Chem. Phys.* **1986**, *85*, 5870−5876.
(98) Röhse, R.; Kutzelnigg, W.; Jaquet, R.; Klopper, W. Potential Energy Surface of the H_3^+ Ground State in the Neighborhood of the Minimum with Micro-Hartree Accuracy and Vibrational Frequencies Derived from It. *J. Chem. Phys.* **1994**, *101*, 2231−2243.

DOI: 10.1021/acs.jpca.5b07718
J. Phys. Chem. A XXXX, XXX, XXX−XXX